Review

Supplementary Materials: Volumetrics of Hydrogen Storage by Physical Adsorption

Sai Smruti Samantaray, Seth T. Putnam, and Nicholas P. Stadie*

*nstadie@montana.edu

Table of Contents

S1. Data Analysis Methodology

All adsorption/desorption equilibria reported in this review were extracted from the original reference in the form of <u>excess adsorption uptake</u> only, using a Java applet (Data Thief III, v 1.7) or by communication directly with the main author(s). The data points are shown as coloured circles (powders) or ×s (pellets) in **Figures 2-6** in the main text and **Figures S1-S26** herein.

The excess uptake data were subsequently fitted to a dual-site Langmuir (DSL) isotherm model (one isotherm at a time) using a squared residuals minimization method (via a nonlinear generalized reduced gradient algorithm):

$$n_e = \left(n_{max} - \rho_{\mathrm{g}}[T, P] \cdot V_{max}\right)\left((1 - \alpha)\left(\frac{K_1 P}{1 + K_1 P}\right) + \alpha\left(\frac{K_2 P}{1 + K_2 P}\right)\right)$$

The fit results are shown as semi-transparent coloured lines in **Figures 2-6** in the main text and **Figures S1-S26** herein. In general, no limitations were imposed on the fitting parameters to obtain the best fit. To reproduce the excess uptake of H_2 on the 9 Å single-layer graphene (SLG) slit pore model reported by Bénard and coworkers,[1] the maximum volume of the adsorbed phase, V_{max}, was imposed as 0.725.

S2. Benchmark Excess H₂ Adsorption Data

2.1. MOF-5 Powder

Five references for H$_2$ adsorption on MOF-5 powder at 77 K are compared in **Figure S1**. The excess uptake reported by Ming and coworkers[2] was ultimately chosen for further analysis in this work.
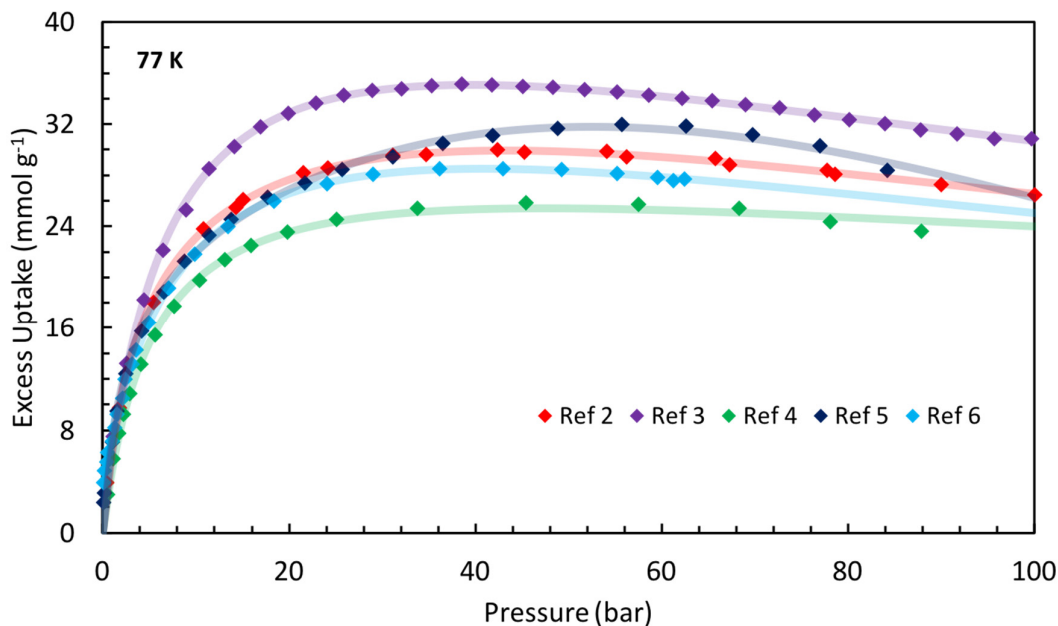
Figure S1. Excess H$_2$ adsorption uptake on MOF-5 powder at 77 K.[2-6]

One reference for H$_2$ adsorption on MOF-5 powder at 298 K was reviewed,[7] as shown in **Figure S2**.
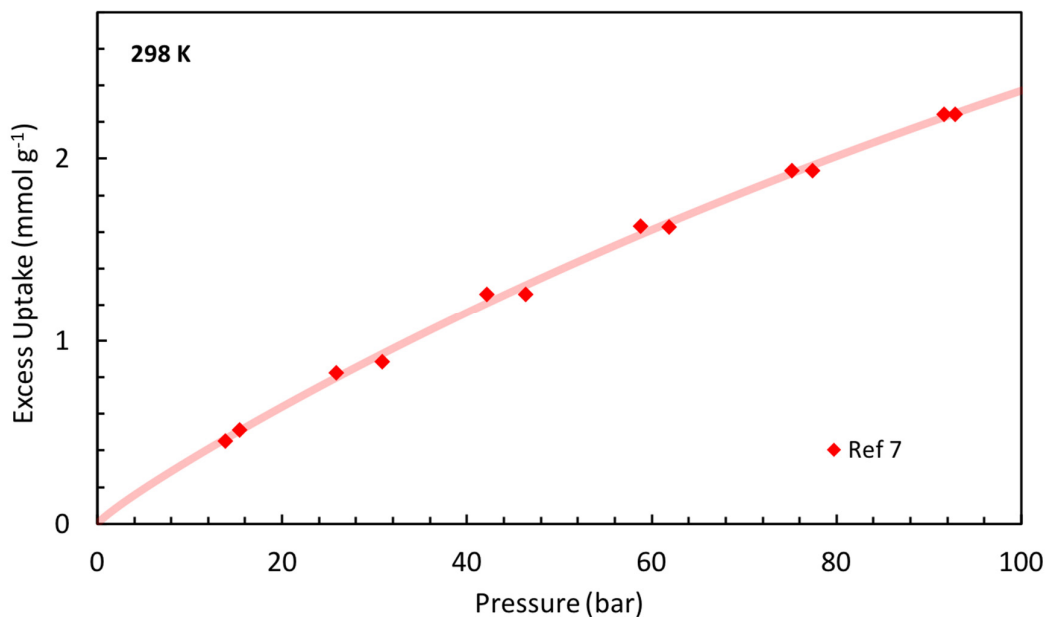
Figure S2. Excess H$_2$ adsorption uptake on MOF-5 powder at 298 K.[7]

2.2. MOF-177 Powder

Two references for H$_2$ adsorption on MOF-177 powder at 77 K are compared in **Figure S3**. The excess uptake reported by Zacharia and coworkers[8] was ultimately chosen for further analysis in this work.
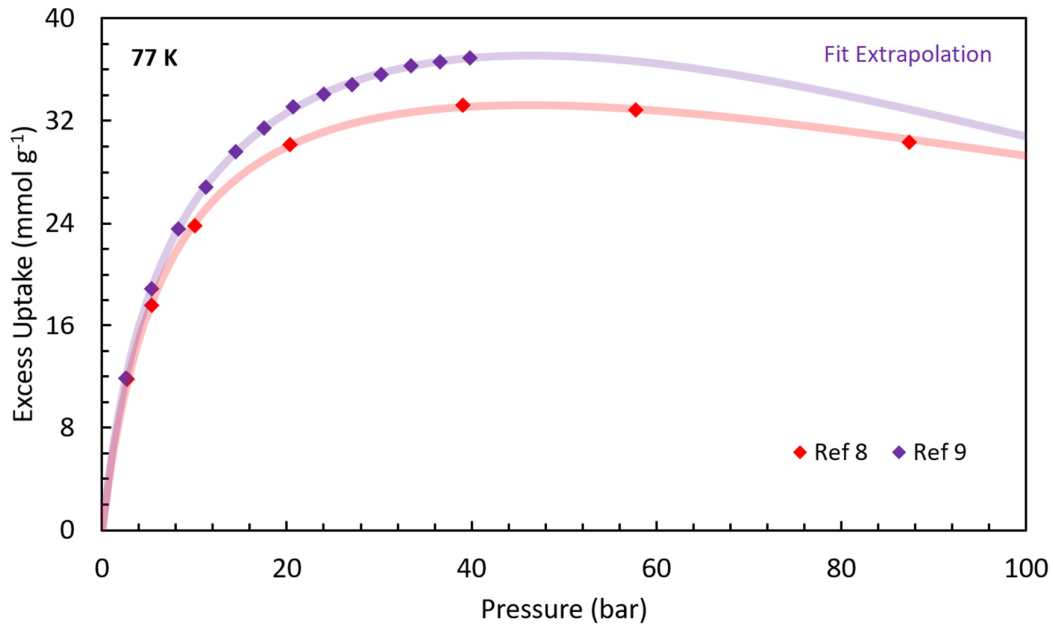
Figure S3. Excess H$_2$ adsorption uptake on MOF-177 powder at 77 K.[8, 9]

Two references for H$_2$ adsorption on MOF-177 powder at 298 K are compared in **Figure S4**. Both measurements are consistent. The excess uptake reported by Zacharia and coworkers[8] was ultimately chosen for further analysis in this work.
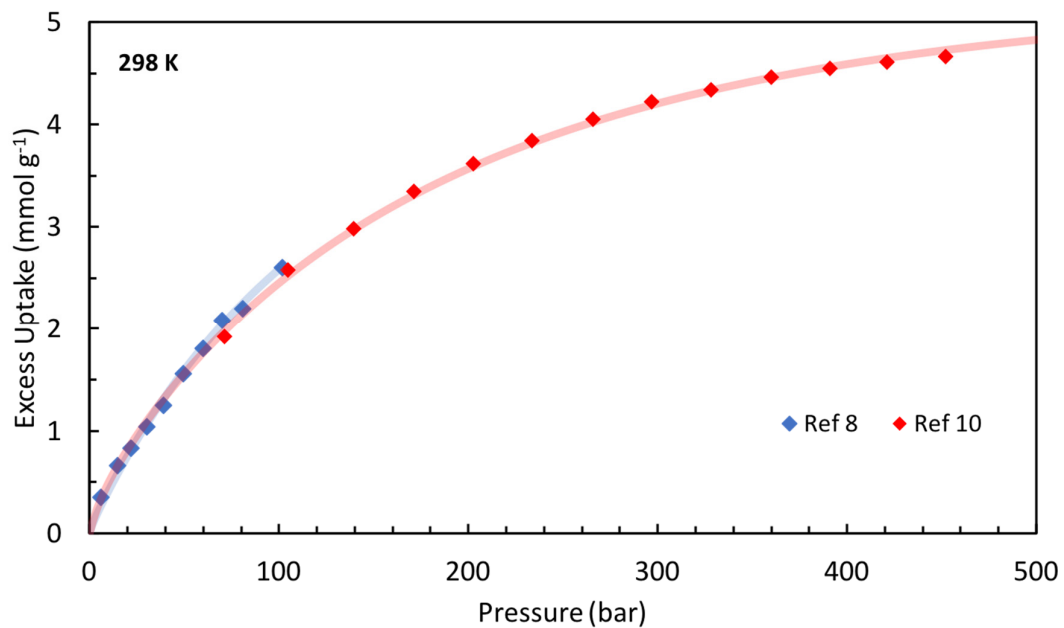
Figure S4. Excess H$_2$ adsorption uptake on MOF-177 powder at 298 K.[8, 10]

2.3. IRMOF-20 Powder

One reference for H_2 adsorption on IRMOF-20 powder at 77 K was reviewed,[11] as shown in **Figure S5**.
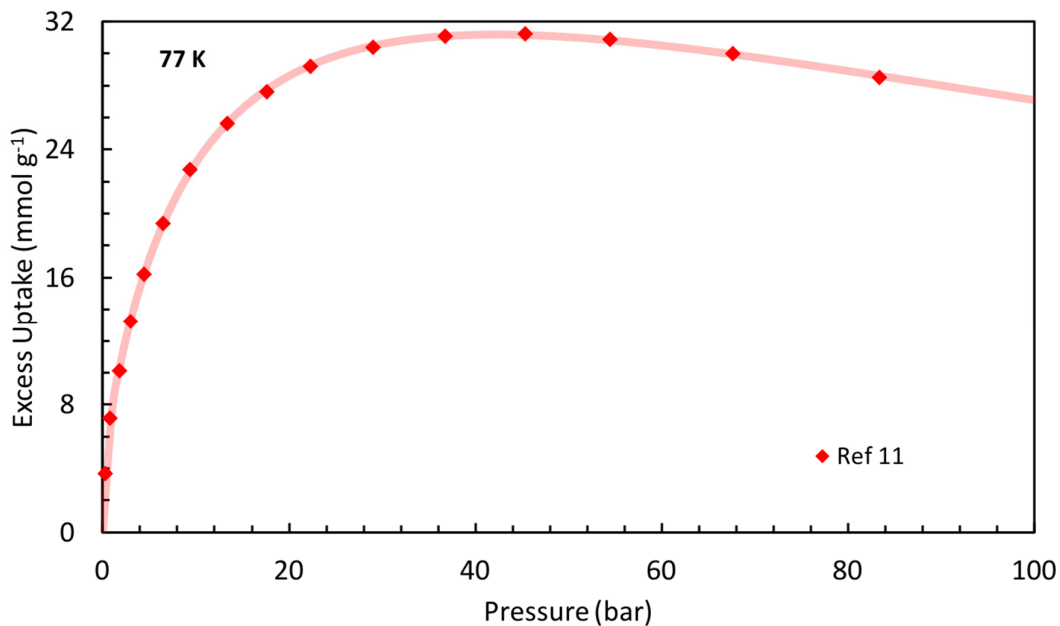
Figure S5. Excess H_2 adsorption uptake on IRMOF-20 powder at 77 K.[11]

Two references for H_2 adsorption on IRMOF-20 powder at 298 K are compared in **Figure S6**. The excess uptake reported by Purewal and coworkers[11] was ultimately chosen for further analysis in this work.
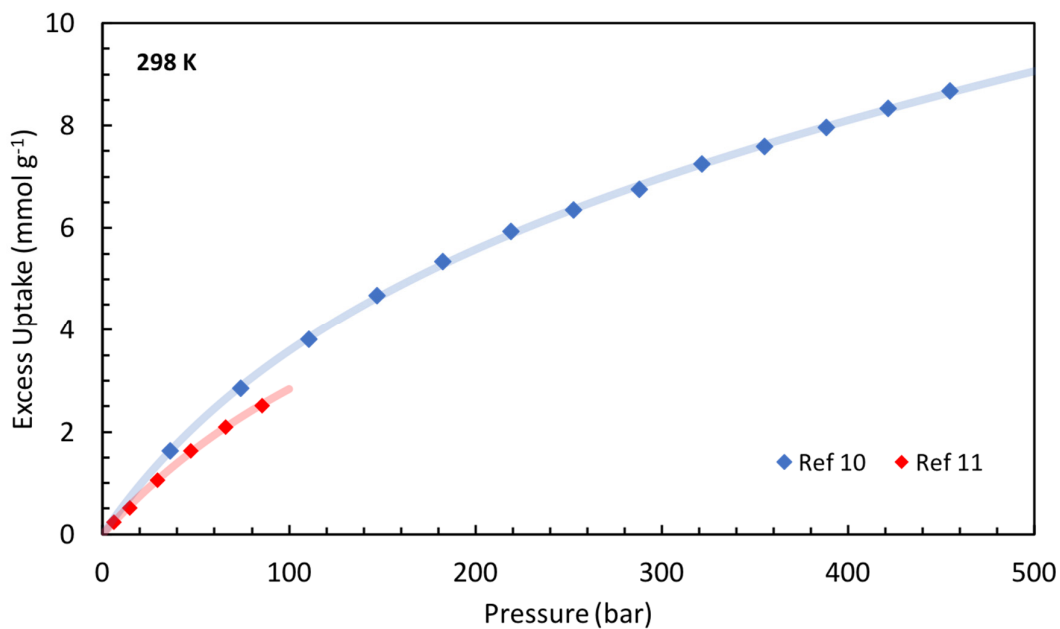
Figure S6. Excess H_2 adsorption uptake on IRMOF-20 powder at 298 K.[10, 11]

2.4. SNU-70 Powder

One reference for H_2 adsorption on SNU-70 powder at 77 K was reviewed,[11] as shown in **Figure S7**.
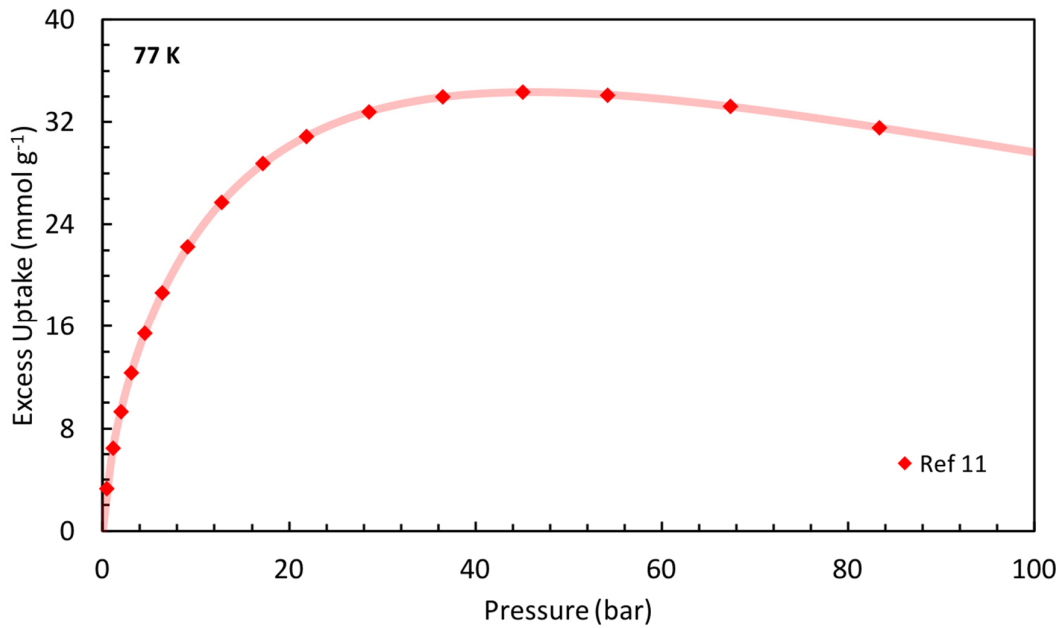
Figure S7. Excess H_2 adsorption uptake on SNU-70 powder at 77 K.[11]

2.5. Ni₂(m-dobdc) Powder

One reference for H_2 adsorption on Ni₂(*m*-dobdc) powder at 298 K was reviewed,[12] as shown in **Figure S8**.
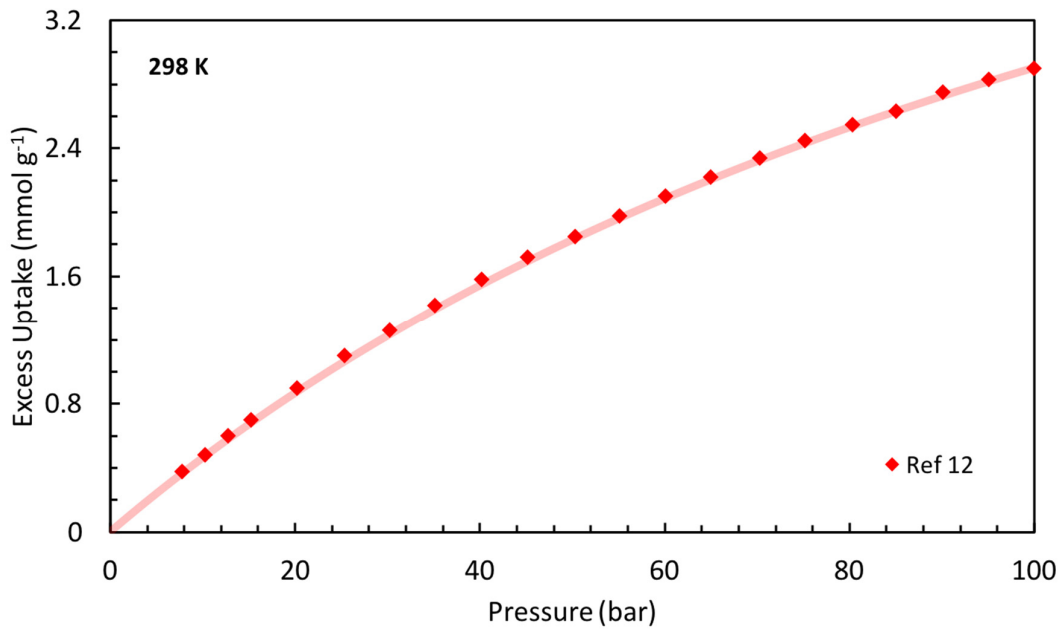
Figure S8. Excess H_2 adsorption uptake on Ni₂(*m*-dobdc) powder at 298 K.[12]

2.6. UiO-66 Powder

One references for H$_2$ adsorption on UiO-66 powder at 77 K was reviewed,[13] as shown in **Figure S9**.
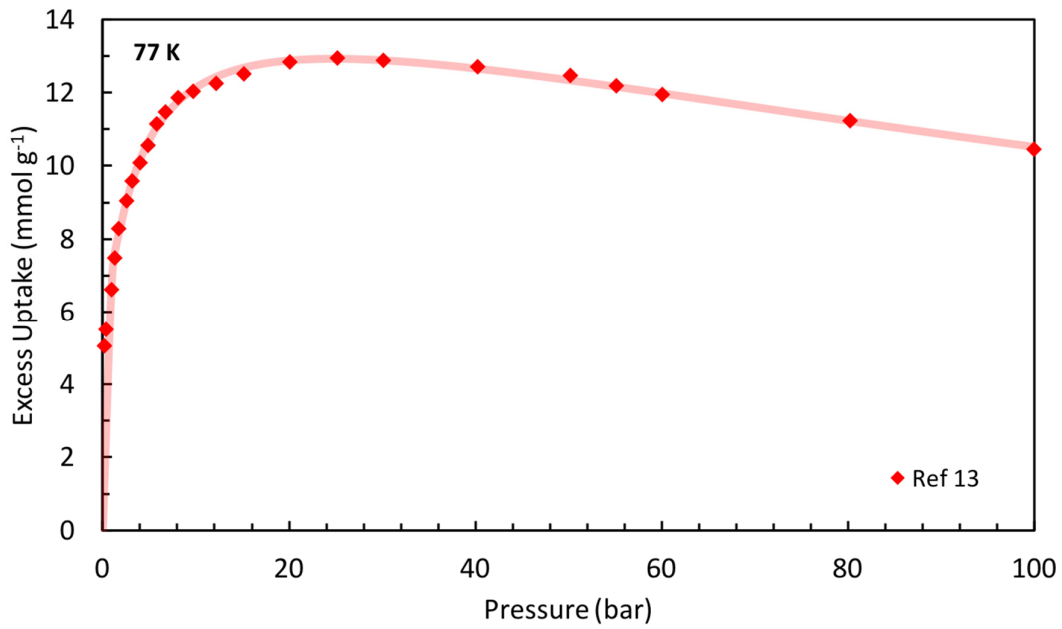
Figure S9. Excess H$_2$ adsorption uptake on UiO-66 powder at 77 K.[13]

One reference for H$_2$ adsorption on UiO-66 powder at 298 K was reviewed,[13] as shown in **Figure S10**.
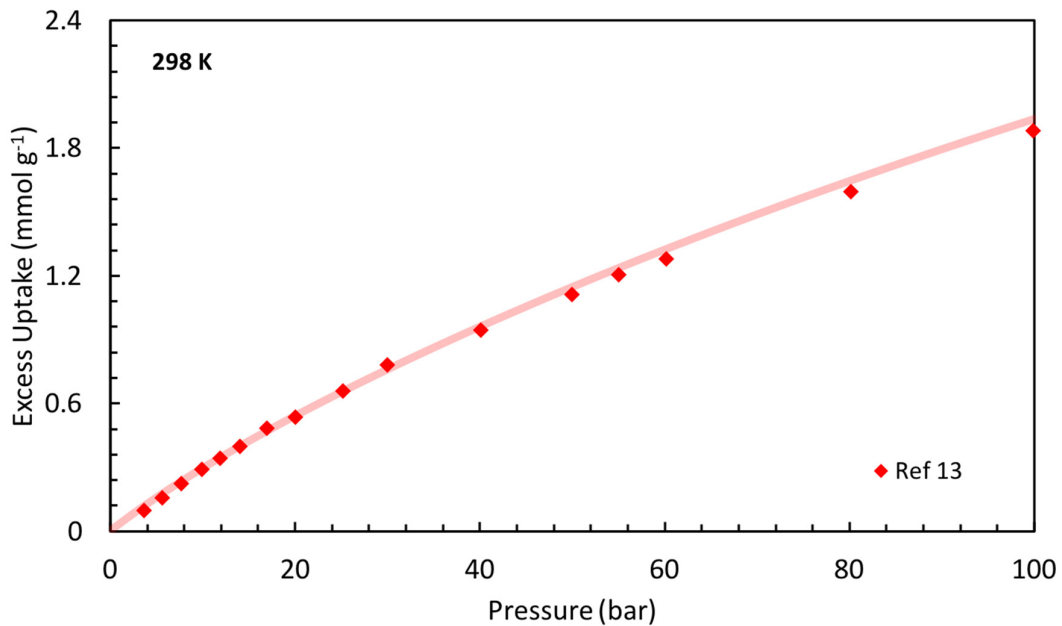
Figure S10. Excess H$_2$ adsorption uptake on UiO-66 powder at 298 K.[13]

2.7. HKUST-1 Powder

Three references for H_2 adsorption on HKUST-1 powder at 77 K are compared in **Figure S11**. The excess uptake reported by García-Holley and coworkers[14] was ultimately chosen for further analysis in this work.
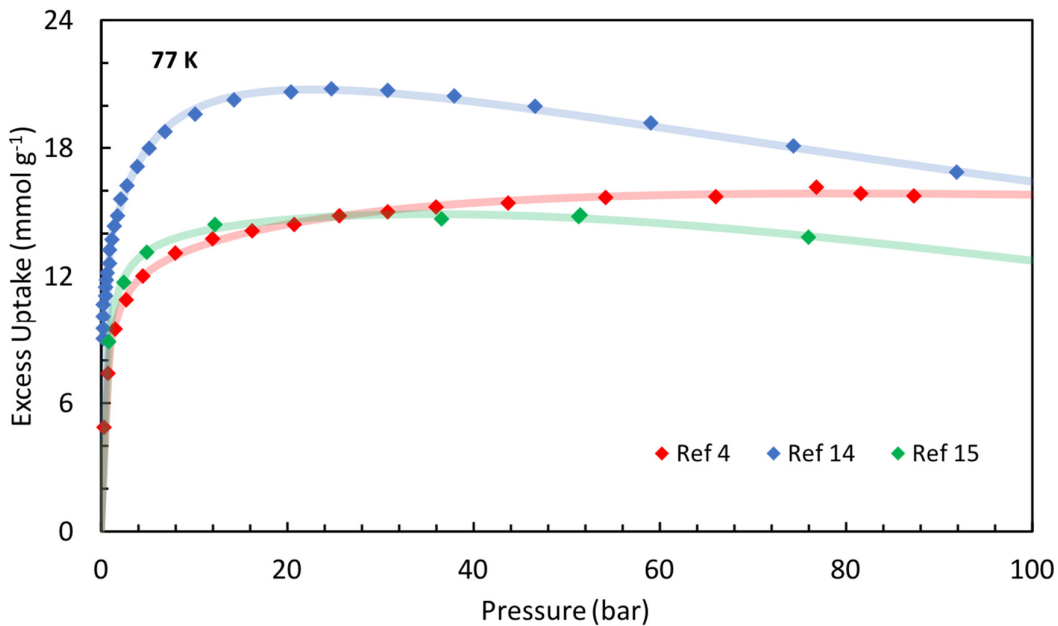
Figure S11. Excess H_2 adsorption uptake on HKUST-1 powder at 77 K.[4, 14, 15]

One references for H_2 adsorption on HKUST-1 powder at 298 K was reviewed,[14] as shown in **Figure S12**.
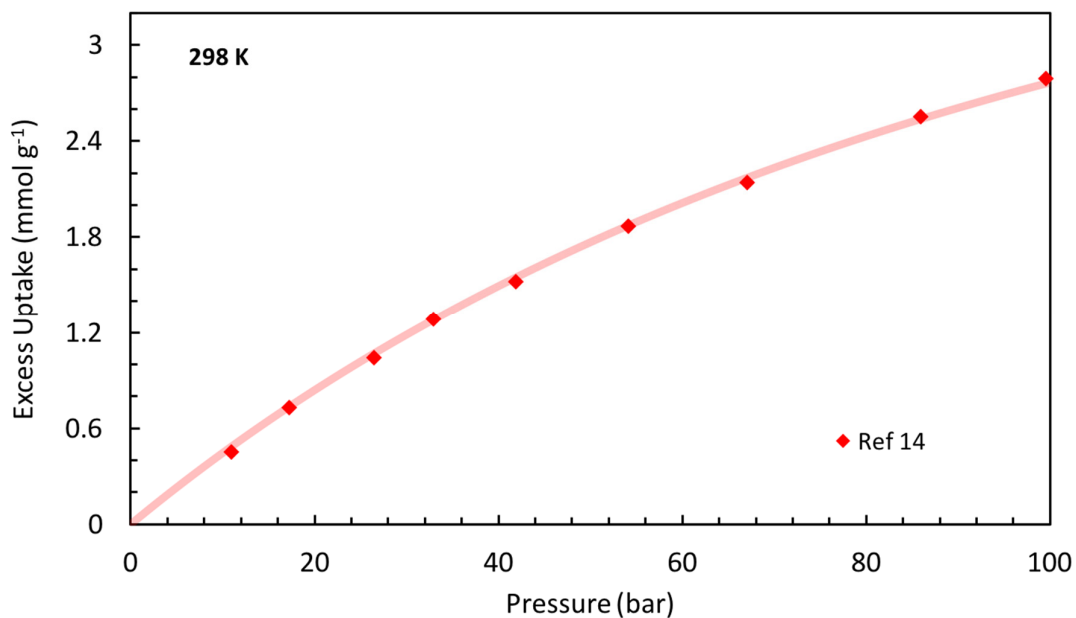
Figure S12. Excess H_2 adsorption uptake on HKUST-1 powder at 298 K.[14]

2.8. Zeolite-Templated Carbon (ZTC) Powder

Two references for H_2 adsorption on faujasite-type ZTC (**FAU**-ZTC) powder at 77 K are compared in **Figure S13**. The excess uptake reported by Geng and coworkers[16] was ultimately chosen for further analysis in this work.
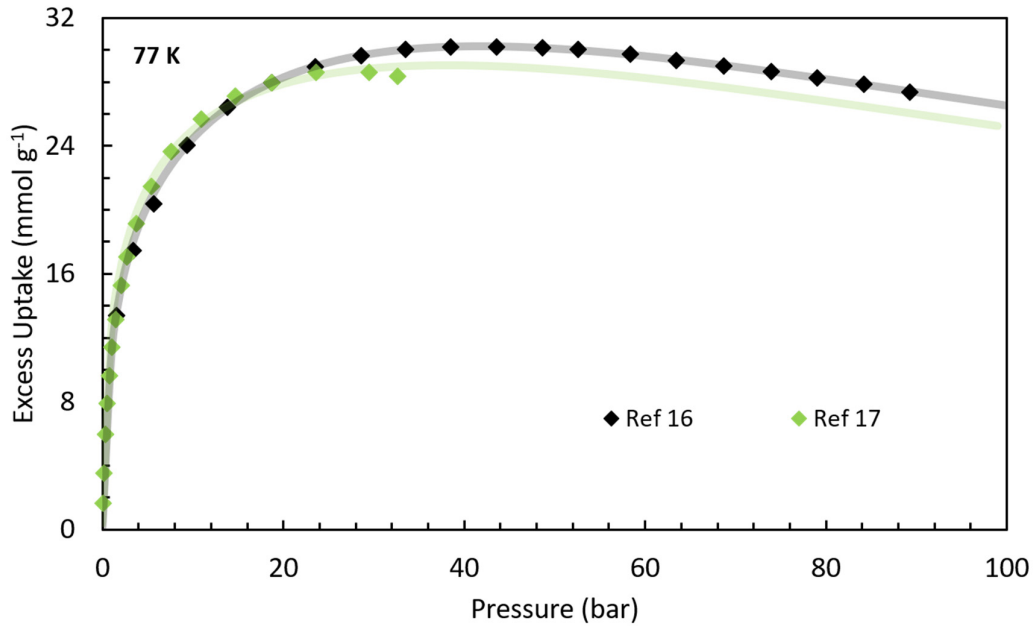
Figure S13. Excess H_2 adsorption uptake on **FAU**-ZTC powder at 77 K.[16, 17]

Four references for H_2 adsorption on faujasite-type ZTC (**FAU**-ZTC) powder at 298 K are compared in **Figure S14**. The excess uptake reported by Gabe and coworkers[18] was ultimately chosen for further analysis in this work.
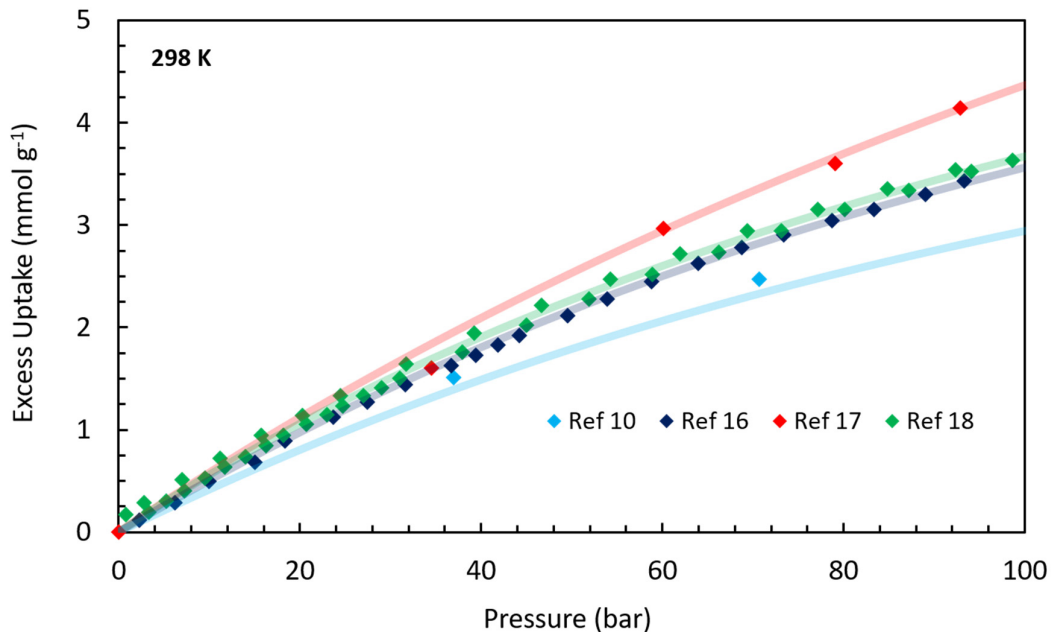
Figure S14. Excess H_2 adsorption uptake on **FAU**-ZTC powder at 298 K.[10, 16-18]

2.9. Zeolite 13X Powder

One reference for H_2 adsorption on Zeolite 13X powder at 77 K was reviewed,[19] as shown in **Figure S15**.
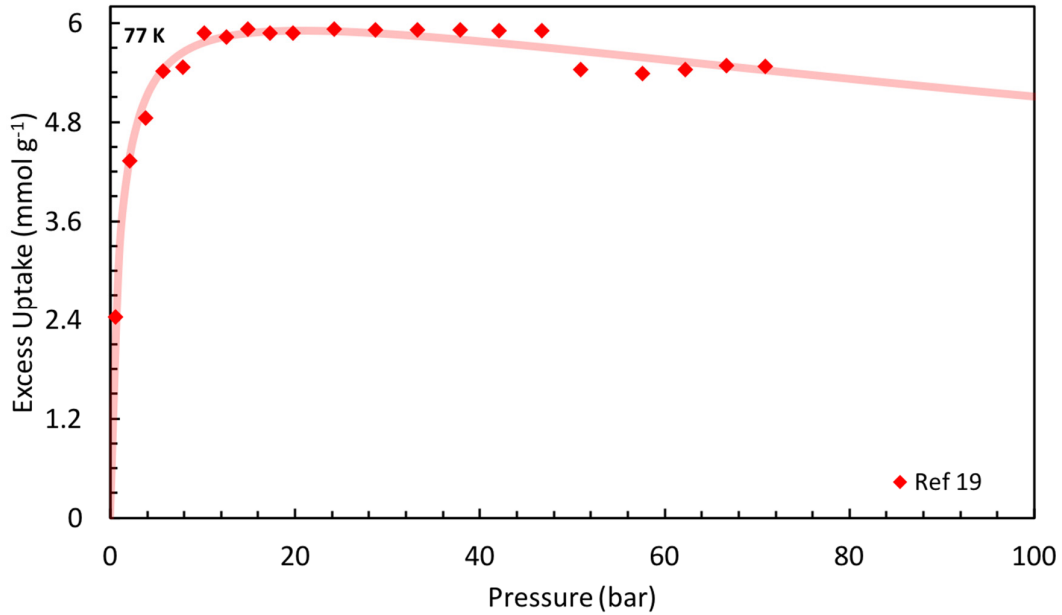
Figure S15. Excess H_2 adsorption uptake on Zeolite 13X powder at 77 K.[19]

One reference for H_2 adsorption on Zeolite 13X powder at 298 K was reviewed, as shown in **Figure S16**.
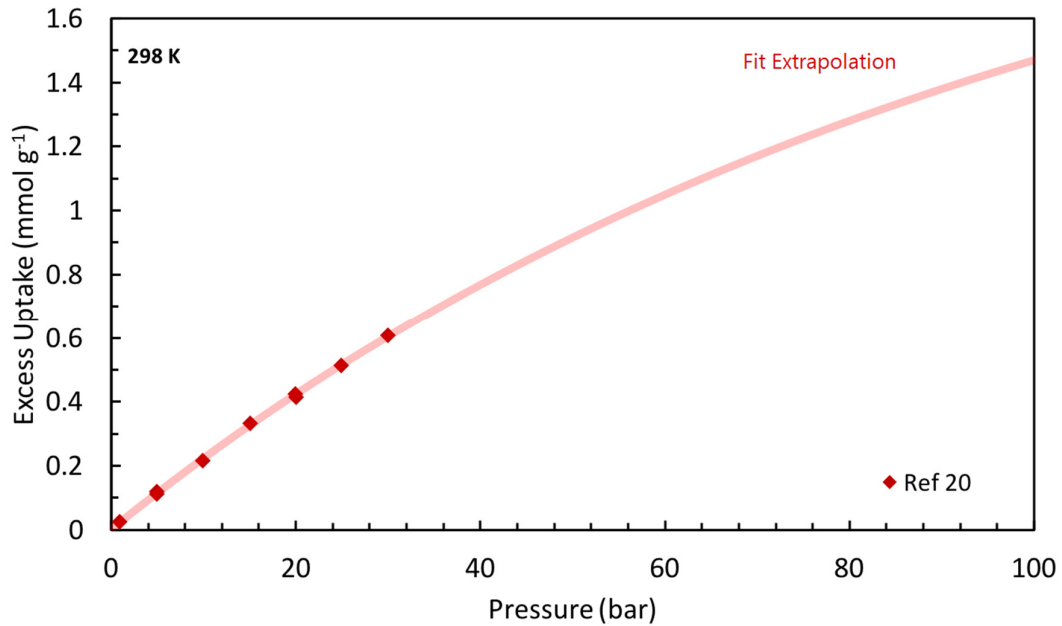
Figure S16. Excess H_2 adsorption uptake on Zeolite 13X powder at 298 K.[20]

2.10. MOF-5 Pellets

One reference for H_2 adsorption on neat MOF-5 pellets at 77 K was reviewed,[7] as shown in **Figure S17**.
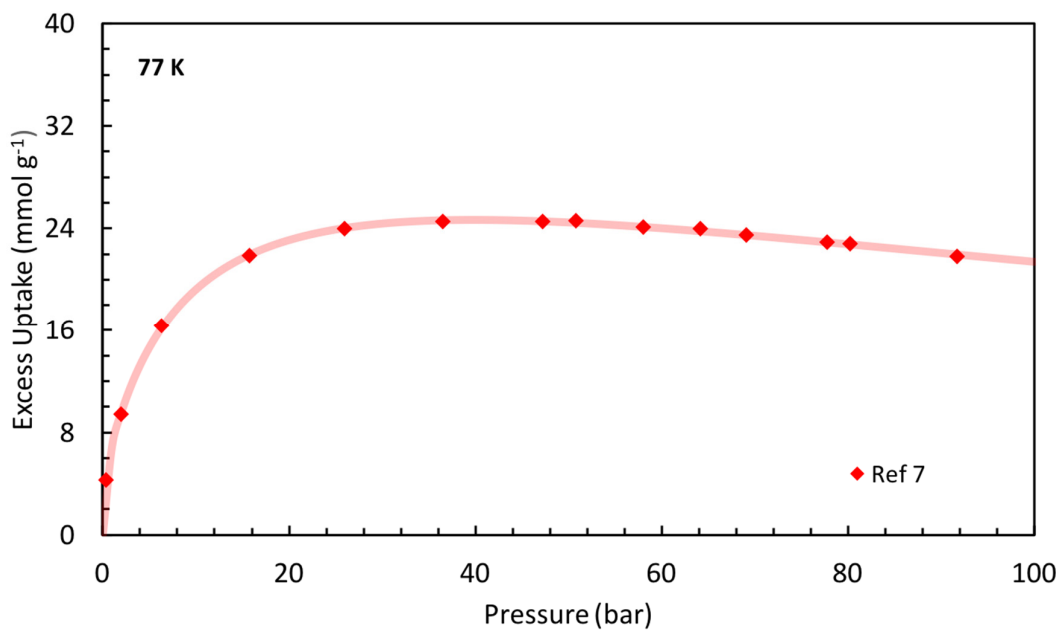
Figure S17. Excess H_2 adsorption uptake on neat MOF-5 pellets at 77 K.[7]

One reference for H_2 adsorption on MOF-5/ENG pellets at 77 K was reviewed,[7] as shown in **Figure S18**.
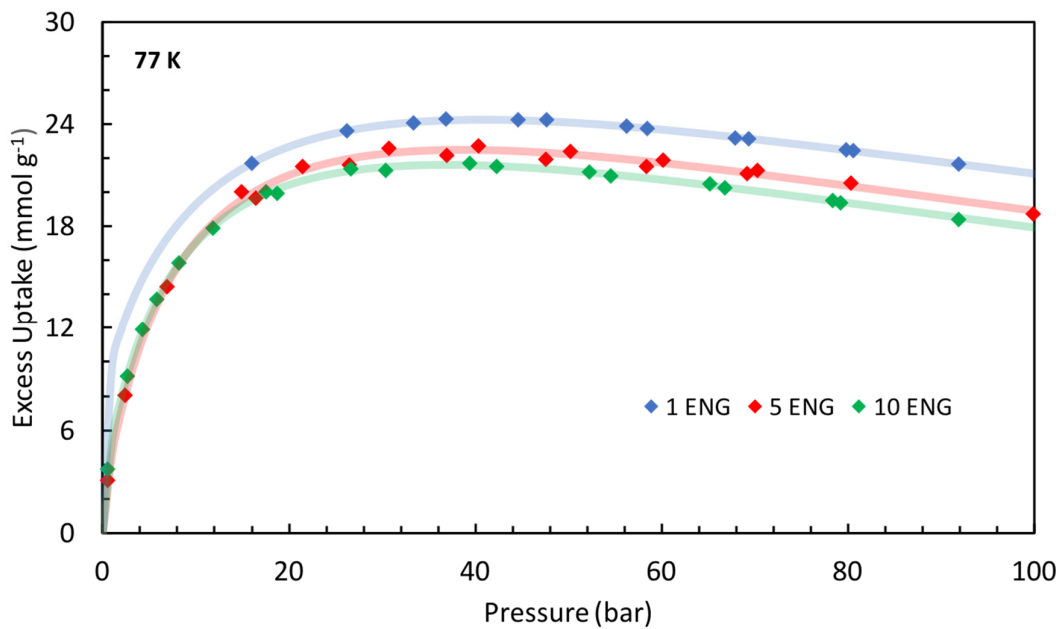
Figure S18. Excess H_2 adsorption uptake on MOF-5/ENG pellets at 77 K.[7]

2.11. MOF-177 Pellets

One reference for H_2 adsorption on neat MOF-177 pellets at 77 K was reviewed,[8] as shown in **Figure S19**.
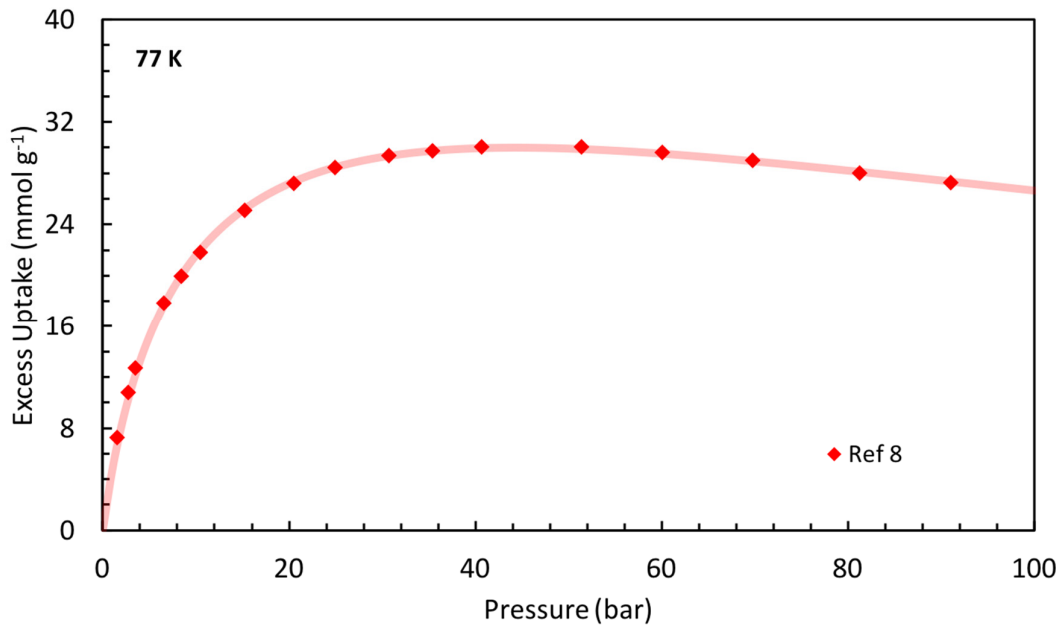
Figure S19. Excess H_2 adsorption uptake on neat MOF-177 pellets at 77 K.[8]

2.12. SNU-70 Pellets

One reference for H_2 adsorption on neat SNU-70 pellets at 77 K was reviewed,[11] as shown in **Figure S20**.
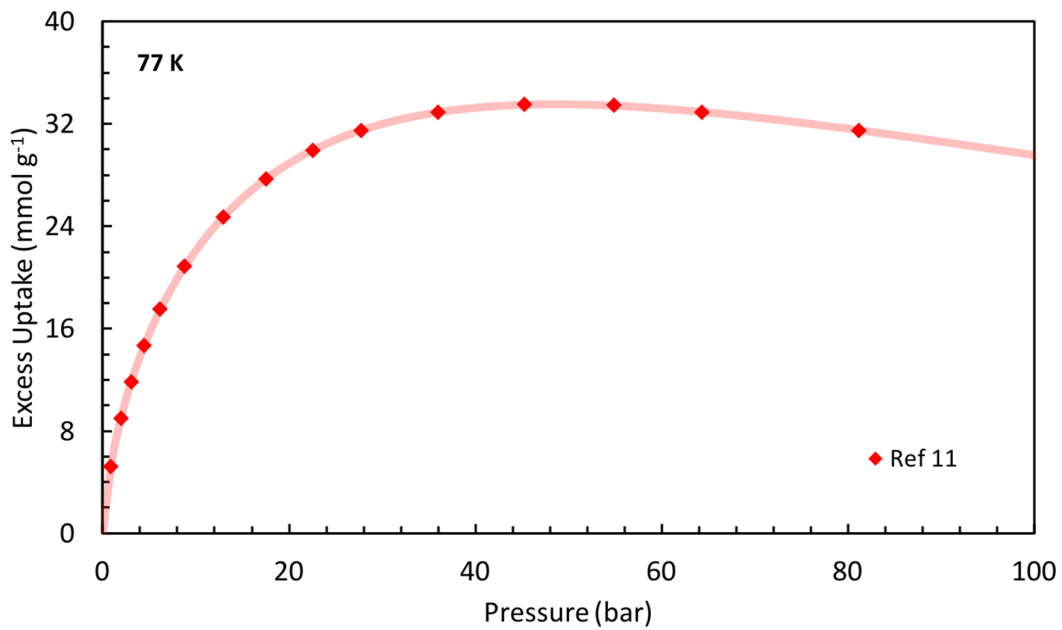
Figure S20. Excess H_2 adsorption uptake on neat SNU-70 pellets at 77 K.[11]

2.13. UiO-66 Pellets

One reference for H$_2$ adsorption on a neat UiO-66 pellet at 77 K was reviewed,[13] as shown in **Figure S21**.
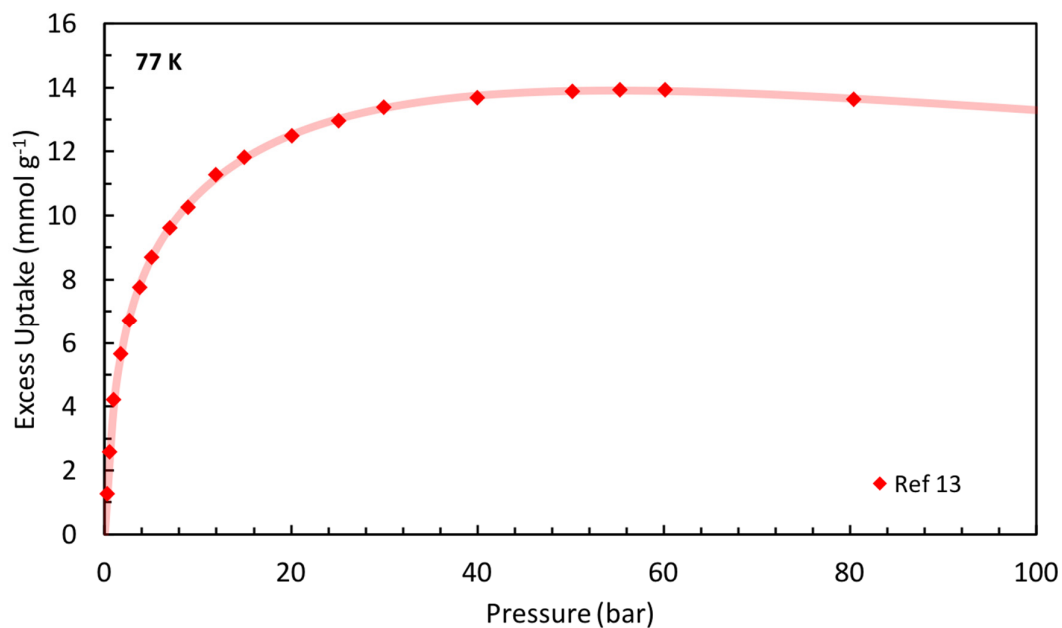
Figure S21. Excess H$_2$ adsorption uptake on a neat UiO-66 pellet at 77 K.[13]

One reference for H$_2$ adsorption on a neat UiO-66 pellet at 298 K was reviewed,[13] as shown in **Figure S22**.
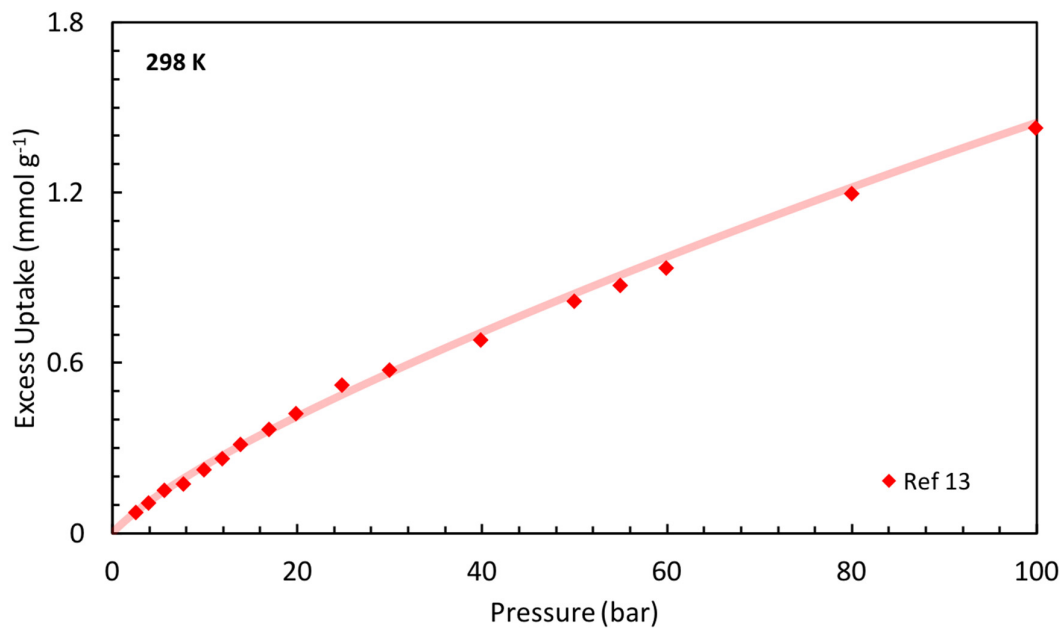
Figure S22. Excess H$_2$ adsorption uptake on a neat UiO-66 pellet at 298 K.[13]

2.14. HKUST-1 Pellets

One reference for H_2 adsorption on neat HKUST-1 pellets at 77 K was reviewed,[15] as shown in **Figure S23**.
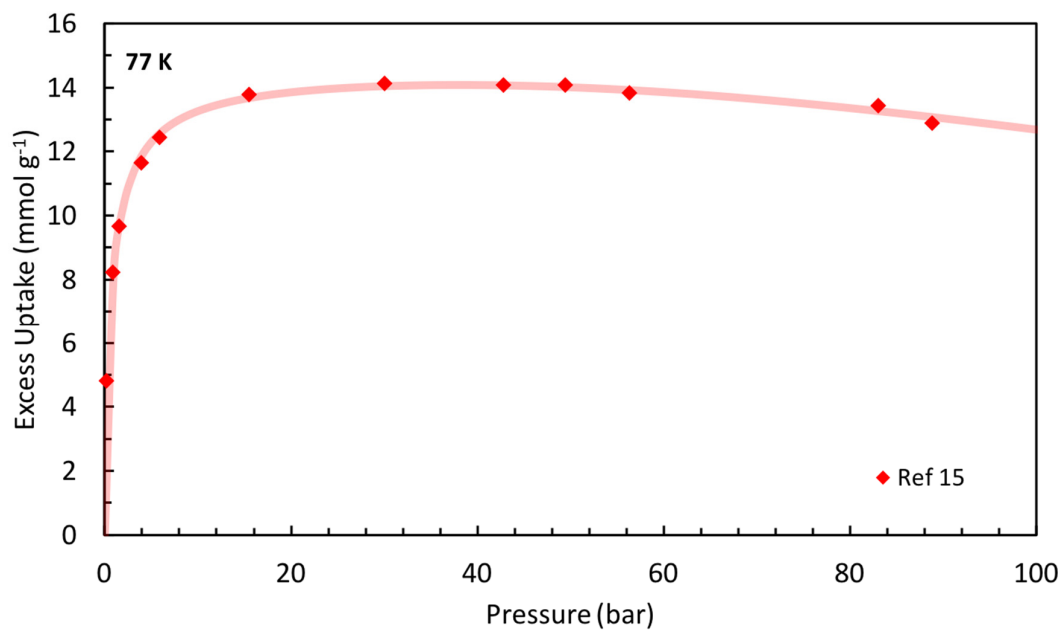
Figure S23. Excess H_2 adsorption uptake on neat HKUST-1 pellets at 77 K.[15]

One reference for H_2 adsorption on neat HKUST-1 pellets at 295 K was reviewed,[15] as shown in **Figure S24**.
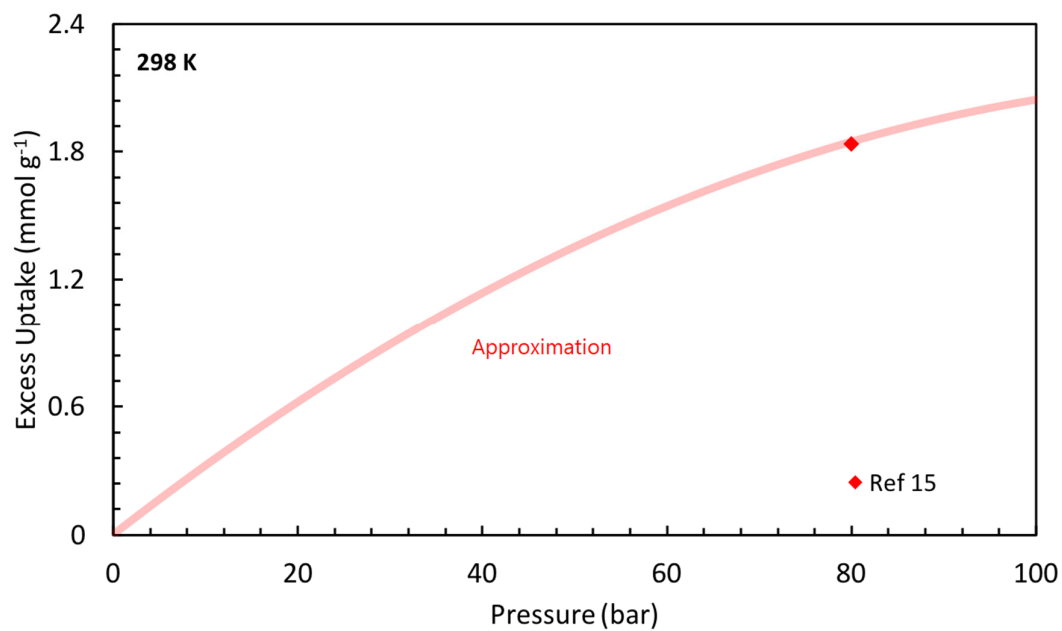
Figure S24. Excess H_2 adsorption uptake on neat HKUST-1 pellets at 295 K (~298 K).[15]

2.15. Zeolite-Templated Carbon (ZTC) Pellets

H_2 adsorption on a ZTC/rGO pellet (based on **FAU**-ZTC) at 77 K is shown in **Figure S25**. The pellet properties are reported elsewhere.[18]
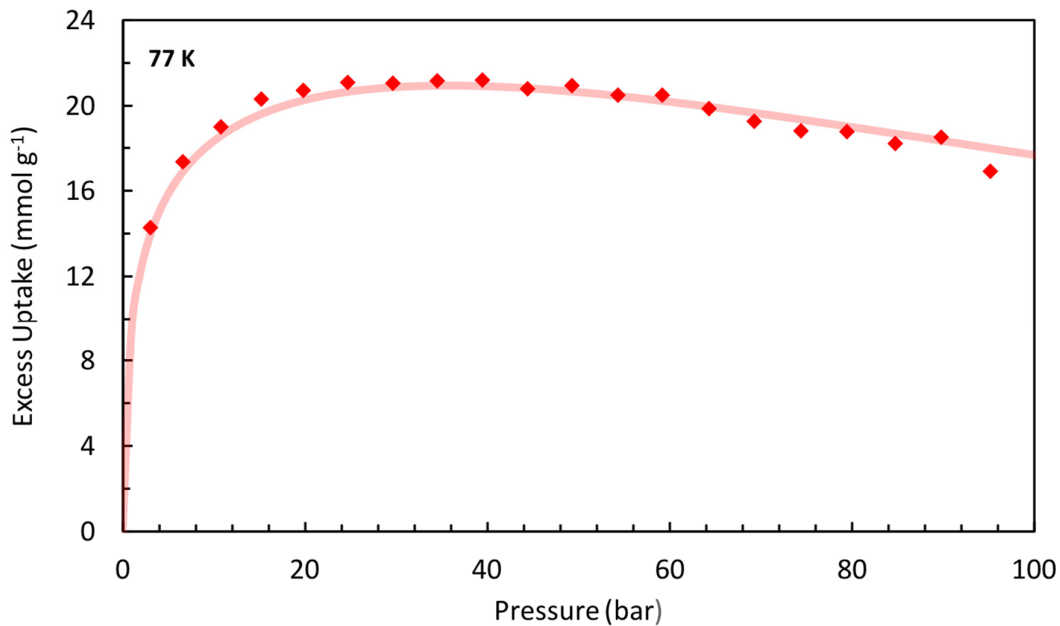
Figure S25. Excess H_2 adsorption uptake on a ZTC/rGO pellet at 77 K.

One reference for H_2 adsorption on a ZTC/rGO pellet (based on **FAU**-ZTC) at 298 K was reviewed,[18] as shown in **Figure S26**.
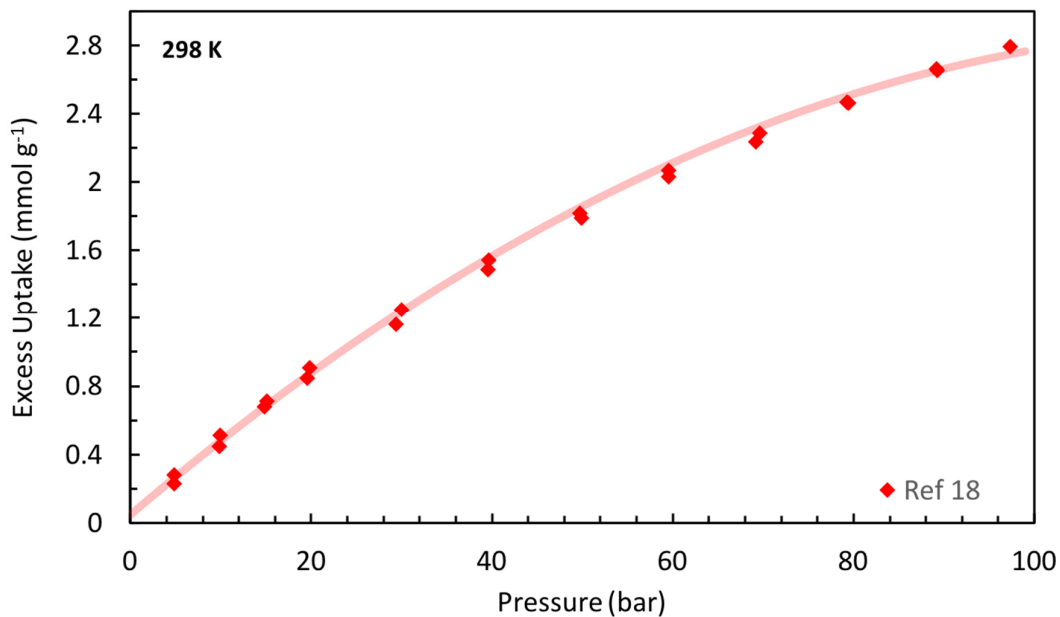
Figure S26. Excess H_2 adsorption uptake on a ZTC/rGO pellet at 298 K.[18]

S3. Crystal Properties

The ideal structural properties of the benchmark MOFs were evaluated using crystallographic data archived within the Cambridge Crystallographic Data Centre (CCDC), Crystallography Open Database (COD)[21], or International Zeolite Association (IZA)[22]. The "most accurate"[23] periodic model of ZTC containing a realistic distribution of O-bearing functional groups (referred to herein as Model II+) was obtained directly from Prof. Hirotomo Nishihara.[24] Each structure was stripped of all solvent and any site disorder, if applicable, prior to structural analysis using the Zeo++ software package (version 0.3).[25] Bulk density was determined directly from the periodic (solvent-free) unit cell. Specific surface area and total pore volume were determined based on the fraction of the unit cell accessible to a spherical probe of radius 0.120 nm, using 2,000 and 200 Monte Carlo samples per cell, respectively. A spherical probe diameter of 0.240 nm mimics that of an H_2 molecule at 77 K,[26] leading to specific surface areas and pore volumes that are ultimately relevant to H_2 adsorption on pristine crystals. For comparison to the measured N_2-accessible surface area, additional calculations were also performed using a spherical probe of radius 0.186 nm, using 2,000 and 200 Monte Carlo samples per cell, otherwise identical to those for the smaller probe. The results are reported in **Tables S1** and **S2**.

Table S1. Crystal Properties of Benchmark MOFs, Zeolites, and ZTC, Accessible to an H_2 Probe (2.40 Å in diameter)

Material	Bulk Density (g mL^{-1})	Skeletal Density (g mL^{-1})	Pore Volume (mL g^{-1})	BET SA (m^2 g^{-1})	BET SA (m^2 mL^{-1})	X_{void} (%)	CIF Reference
MOF-5**	0.5992	2.7334	1.3030	3733	2237	78.08%	average**
MOF-177	0.4256	2.1461	1.8836	4541	1933	80.17%	230642 (CCDC)
IRMOF-20	0.5110	1.8405	1.4135	3559	1819	72.24%	4101152 (COD)
SNU-70	0.4005	2.4081	2.0816	4862	1947	83.37%	846935 (CCDC)
UiO-66	1.2348	2.6286	0.4294	2135	2636	53.02%	733458 (CCDC)
HKUST-1	0.8791	2.8222	0.7832	2718	2402	68.16%	112954 (CCDC)
Ni$_2$(*m*-dobdc)	1.2510	3.0437	0.4708	1488	1861	58.90%	authors[12]
*BEA	1.5284	2.629	0.2739	1157	1768	41.86%	***BEA** (IZA)
EMT	1.3291	2.423	0.3397	1149	1527	45.15%	**EMT** (IZA)
FAU	1.3278	2.435	0.3425	1160	1541	45.48%	**FAU** (IZA)
LTA	1.4143	2.395	0.2986	1144	1618	40.96%	**LTA** (IZA)
MFI	1.8382	2.575	0.1557	763	1402	28.62%	**MFI** (IZA)
FAU-ZTC	0.4626	1.9146	1.6394	4374	2023	75.84%	authors[24]

**MOF-5 is reported herein as the average of two experimental CIFs: 256965 (CCDC) and 1516287 (COD)

Table S2. Crystal Properties of Benchmark MOFs, Zeolites, and ZTC, Accessible to an N_2 Probe (3.72 Å in diameter)

Material	Bulk Density (g mL^{-1})	Skeletal Density (g mL^{-1})	Pore Volume (mL g^{-1})	BET SA (m^2 g^{-1})	BET SA (m^2 mL^{-1})	X_{void} (%)	CIF Reference
MOF-5**	0.5992	2.549	1.2765	3633	2177	76.49%	average**
MOF-177	0.4256	2.055	1.8629	4590	1954	79.29%	230642 (CCDC)
IRMOF-20	0.5110	1.750	1.3855	3495	1786	70.81%	4101152 (COD)
SNU-70	0.4005	2.192	2.0407	4784	1916	81.73%	846935 (CCDC)
UiO-66	1.2348	2.283	0.3719	1047	1292	45.92%	733458 (CCDC)
HKUST-1	0.8837	2.407	0.7161	2026	1790	63.28%	112954 (CCDC)
Ni$_2$(*m*-dobdc)	1.2510	2.906	0.4553	1194	1494	56.96%	authors[12]
*BEA	1.5284	2.576	0.2661	874	1335	40.67%	***BEA** (IZA)
EMT	1.3291	2.399	0.3356	961	1277	44.60%	**EMT** (IZA)
FAU	1.3278	2.410	0.3382	972	1290	44.91%	**FAU** (IZA)
LTA	1.4143	2.348	0.2811	741	1048	39.76%	**LTA** (IZA)
MFI	1.8382	2.454	0.1365	364	670	25.09%	**MFI** (IZA)
FAU-ZTC	0.4626	1.815	1.611	4295	1987	74.51%	authors[24]

****MOF-5 is reported herein as the average of two experimental CIFs: 256965 (CCDC) and 1516287 (COD)

The crystal properties of the five single-layer graphene (SLG) slit pore models investigated by Bénard and coworkers[1] are shown in **Table S3**. The unit cells were constructed by extending the lattice parameter, *c*, of graphite. Identical methods were used to determine the pore volume and surface area as for the MOFs, zeolites, and ZTC in **Tables S1-S2**.

Table S3. Crystal Properties of SLG Slit Pore Models, Accessible to an H_2 Probe (2.40 Å in diameter)

Model	Slit Spacing (Å)	Bulk Density (g mL^{-1})	Skeletal Density (g mL^{-1})	Pore Volume (mL g^{-1})	BET SA (m^2 g^{-1})	BET SA (m^2 mL^{-1})	X_{void} (%)	Reference
SLG9Å	9	0.8484	2.2033	0.7248	2961	2512	61.49%	this work
SLG12Å	12	0.6363	2.2031	1.1177	2961	1884	71.12%	this work
SLG15Å	15	0.5090	2.1771	1.5052	2961	1507	76.62%	this work
SLG18Å	18	0.4242	2.2028	1.9035	2961	1256	80.74%	this work
SLG20Å	20	0.3818	2.2448	2.1739	2961	1130	82.99%	this work

S4. Powder and Pellet Properties

Powder and pellet properties from several benchmark MOFs, carbons, and zeolites were retrieved and analyzed as part of this review, as summarized in **Tables S4** and **S5**. Note: surface areas and pore volumes are shown "as reported" with no attempt made to regularize their analysis.

Table S4. Powder and Densified Powder Properties of Benchmark MOFs and ZTC

Material	Method	Bulk Density (g mL^{-1})	Skeletal Density (g mL^{-1})	Pore Volume (mL g^{-1})	BET SA (m^2 g^{-1})	BET SA (m^2 mL^{-1})	He X$_{void}$ (%)	Reference
MOF-5	Tapped	0.13	2.03	1.27	2763	359	94%	[2]
MOF-5	Jolted	0.22	2.03	1.27	2763	608	89%	[2]
MOF-177	Tapped	0.21	1.56	1.74	4143	858	87%	[8]
MOF-177	Tapped	0.25	1.5	1.67	4126	1019	83%	[10]
IRMOF-20	Tapped	0.20	1.6	1.67	3689	738	88%	[10]
SNU-70	Tapped	0.20	1.95	2.03	4944	989	90%	[11]
UiO-66	Tapped	0.57	1.65	0.96	1737	990	65%	[13]
HKUST-1	Tapped	0.31	1.9	0.57	1290	396	84%	[10]
Zeolite 13X	Tapped	0.595	2.36	NR	NR	NR	75%	[20]
FAU-ZTC	Tapped	0.19	1.75	1.70	3792	720	89%	this work
FAU-ZTC	Tapped	0.12	1.9	2.21	3035	358	94%	[10]

NR – not reported

Table S5. Select Pellet Properties of Benchmark MOFs and ZTC

Material	Binder	Bulk Density (g mL^{-1})	Skeletal Density (g mL^{-1})	Pore Volume (mL g^{-1})	BET SA (m^2 g^{-1})	BET SA (m^2 mL^{-1})	X$_{void}$ (%)	Reference
MOF-5	Neat	0.52	2.03	1.12	2263	1177	74%	[7]
MOF-5	1% ENG	0.49	2.03	1.12	2584	1266	76%	[7]
MOF-5	5% ENG	0.47	2.03	1.14	2623	1233	77%	[7]
MOF-5	10% ENG	0.48	2.03	1.06	2413	1156	76%	[7]
MOF-177	Neat	0.39	1.56	1.62	4029	1551	75%	[8]
SNU-70	Neat	0.24	1.95	NR	NR	NR	88%	[11]
UiO-66	Neat	1.45	1.78	0.81	1707	2475*	13%*	[13]
HKUST-1	Neat	0.86	NR	0.53	1189	1023	NR	[15]
FAU-ZTC	5% rGO	0.67	1.69	1.35	2585	1732	60%	[18]

NR – not reported
*seemingly unphysical

S5. Common vs. Skeletal vs. Swollen Approximations

The volumetric total quantity of H_2 adsorbed, as generally defined by Equation 7, is subject to discrepancy on the basis of the source of information used to determine the bulk volume, V_{bulk}, and void fraction, X_{void}, of the adsorbent. Section 2.3 in the main text gives a description of three commonly employed pairs of information used to determine the volumetric storage quantity, given by Equations 8-10. An example of the discrepancy between these quantities is shown in **Figures 2b-2c**; the discrepancy is extremely large owing to the problematic assumption that the total pore volume of a powder (in this case, MOF-5) is equal to the total void volume of the powder when packed at tap density within a container. Hence, both the common and swollen approximations are inappropriate for powders.

However, the common approximation is very often employed in the analysis of monoliths and pellets. Two representative examples of the discrepancy that still exists between the three approximations when applied to pelletized samples of MOF-5[7] are shown in **Figures S27-S28**.
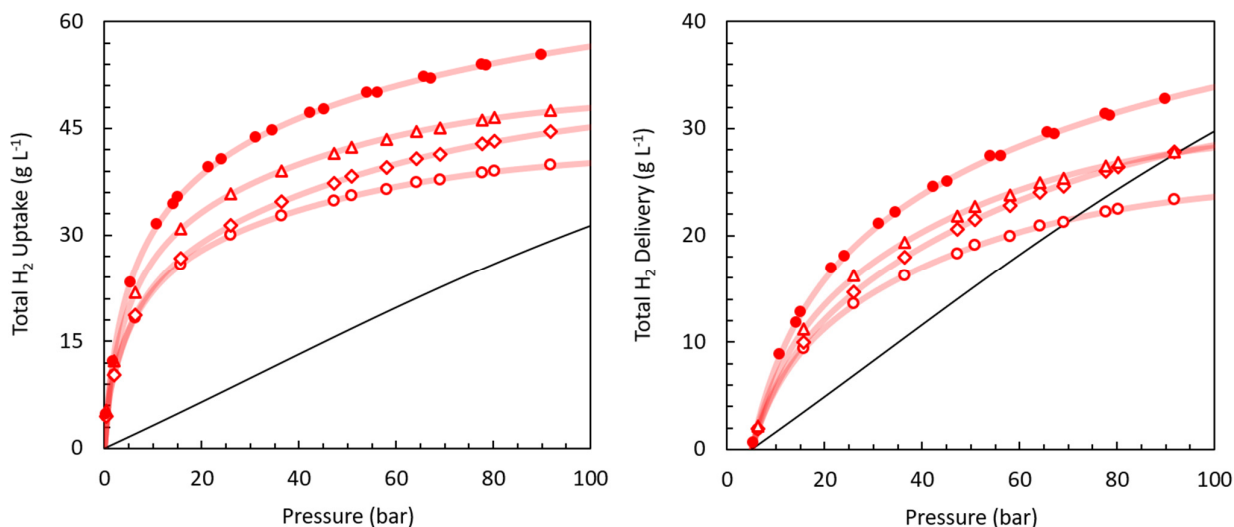
Figure S27. Total H_2 uptake and delivery on a neat MOF-5 pellet at 77 K under three different assumptions: common (circle), skeletal (diamond), and swollen (triangle). The crystalline assumption for MOF-5 (filled circle) is shown for comparison.[7]
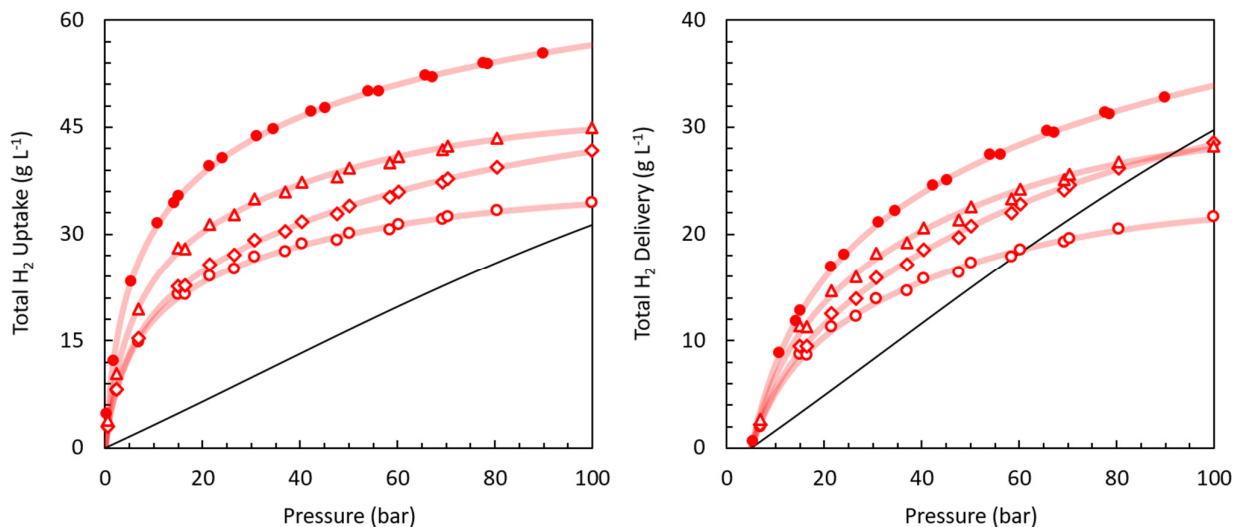
Figure S28. Total H_2 uptake and delivery on a MOF-5/ENG pellet at 77 K under three different assumptions: common (circle), skeletal (diamond), and swollen (triangle). The crystalline assumption for MOF-5 (filled circle) is shown for comparison.[7]

S6. Porous Carbon Comparison

The excess gravimetric H_2 uptake on selected porous carbon powders at 77 K and 298 K is shown in **Figures S29** and **S30**, respectively.[27]. The materials are referenced by a short name followed by a number corresponding to the reported BET surface area: ZTC3806[18], CA3771[28], AX2664, MSC3476, KUA2887, and ZTC3035[10], MSC3420[29], MSC3244 and ZTC3591[17], MSC2680 and ZTC3800[30], MSC3305, MSP2363, and SA2204[31], and CAC3711 and ZTC3751[16], the latter of which is referred to elsewhere herein simply as "ZTC" or "**FAU**-ZTC".
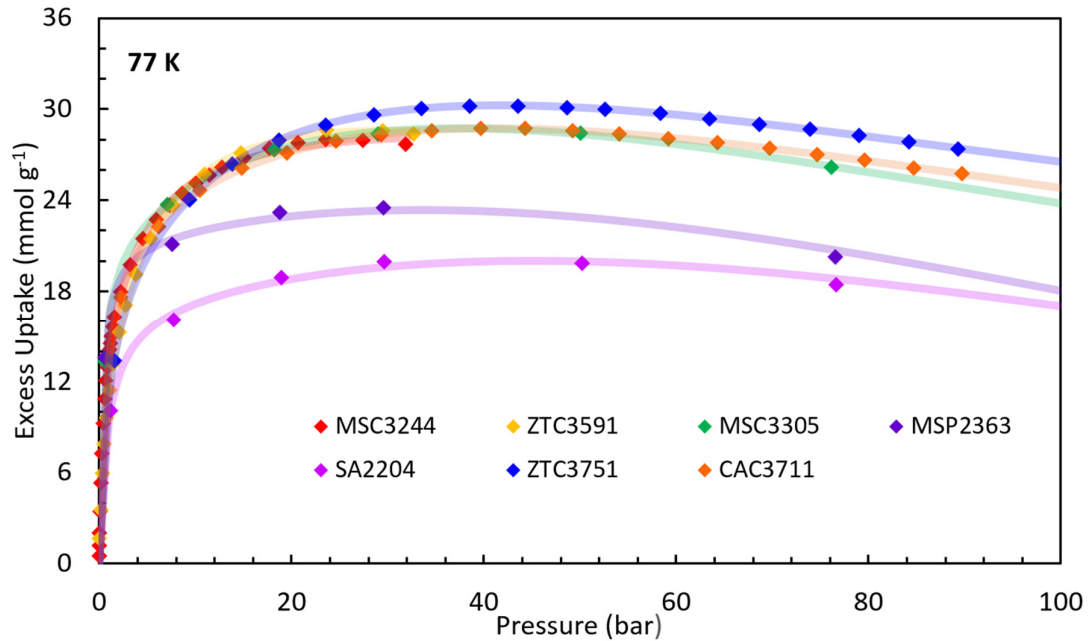
Figure S29. Excess H_2 adsorption uptake on porous carbon powders at 77 K.
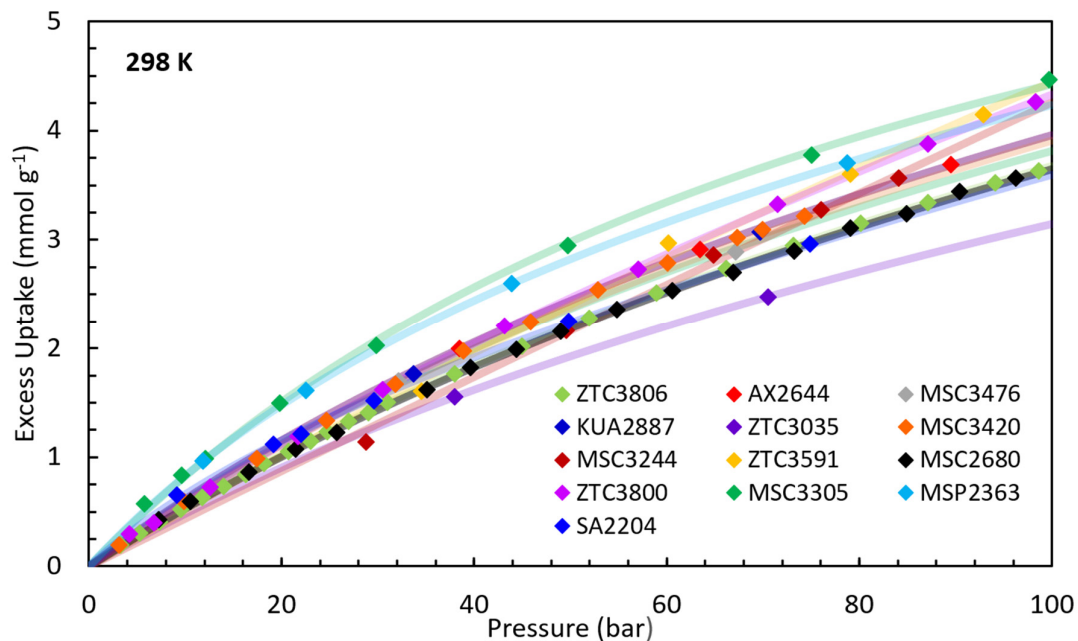
Figure S30. Excess H_2 adsorption uptake on porous carbon powders at 298 K.

The total volumetric H_2 storage and delivery by porous carbon powders depends significantly on packing density; a controlled comparison is shown in **Figures S31** and **S32** where, purely for sake of apples-to-apples analysis, the packing density is fixed at 0.2 g mL^{-1}, the skeletal density is fixed at 2.1 g mL^{-1}, and the skeletal approximation is employed. This is merely an approximation and it is well-recognized that the tap density of carbon powders varies with gravimetric surface area (as shown by the grey ×s in **Figure 3a**). Therefore, it must be emphasized that the calculations of H_2 delivery shown in **Figures S31** and **S32** are to be interpreted with caution.
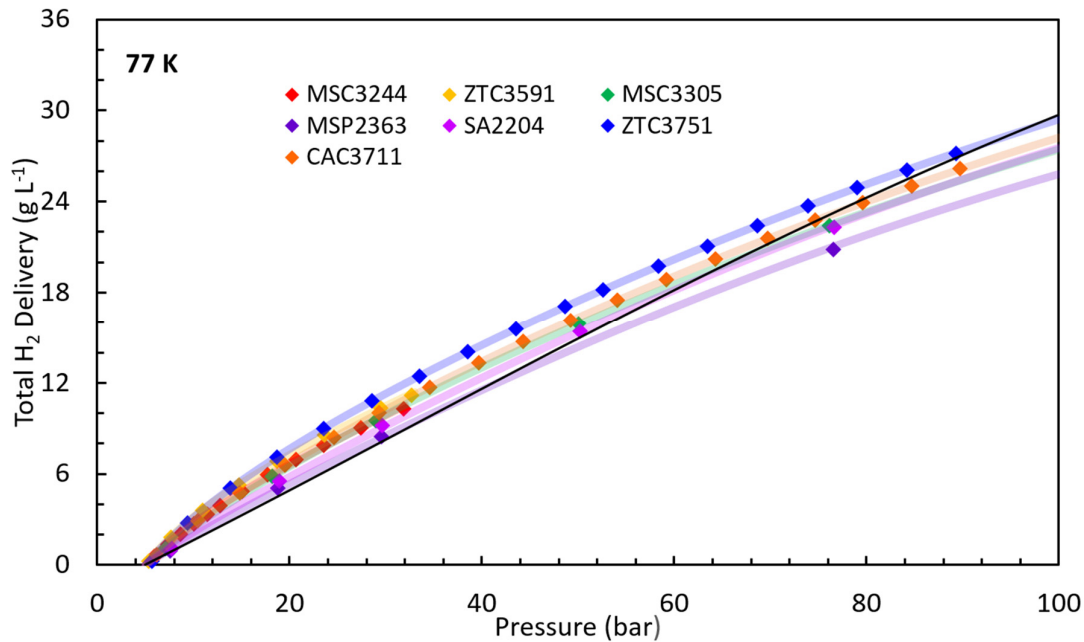
Figure S31. Total H_2 delivery on porous carbon powders (ρ_{bulk} = 0.2 g mL^{-1}, ρ_{skel} = 2.1 g mL^{-1}) at 77 K.
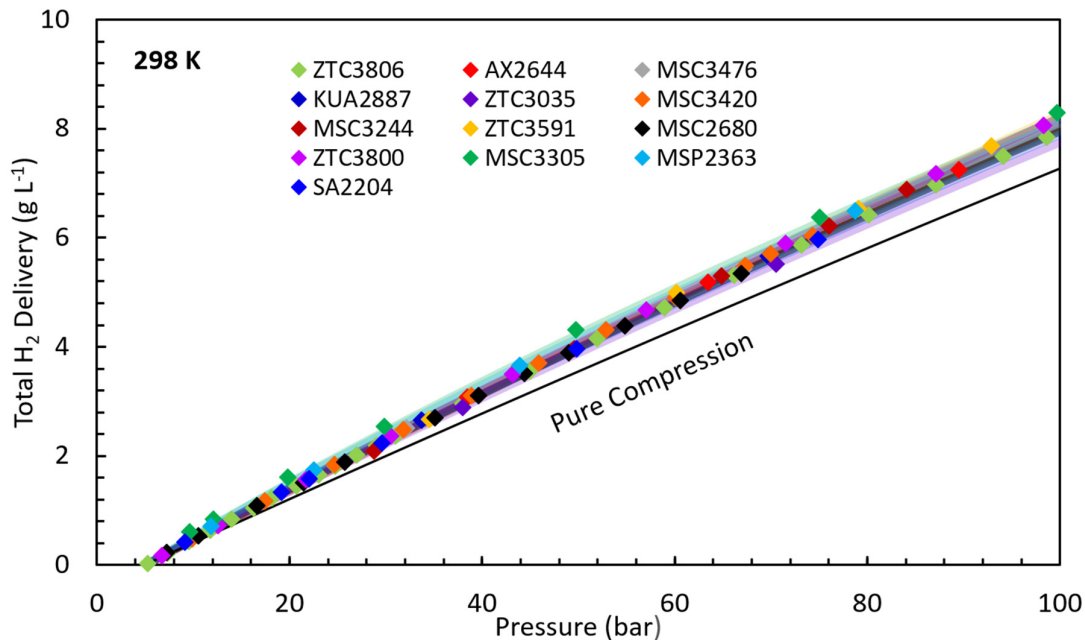
Figure S32. Total H_2 delivery on porous carbon powders (ρ_{bulk} = 0.2 g mL^{-1}, ρ_{skel} = 2.1 g mL^{-1}) at 298 K.

S7. Supporting References

1.   Bénard, P.; Chahine, R.; Chandonia, P.; Cossement, D.; Dorval-Douville, G.; Lafi, L.; Lachance, P.; Paggiaro, R.; Poirier, E., Comparison of hydrogen adsorption on nanoporous materials. *J. Alloys Compd.* **2007,** *446*, 380-384.

2.   Ming, Y.; Purewal, J.; Sudik, A.; Xu, C.; Yang, J.; Veenstra, M.; Rhodes, K.; Soltis, R.; Warner, J.; Gaab, M., Thermophysical properties of MOF-5 powders. *Microporous Mesoporous Mater.* **2014,** *185*, 235-244.

3.   Kaye, S. S.; Dailly, A.; Yaghi, O. M.; Long, J. R., Impact of preparation and handling on the hydrogen storage properties of $Zn_4O(1, 4$-benzenedicarboxylate$)_3$ (MOF-5). *J. Am. Chem. Soc.* **2007,** *129* (46), 14176-14177.

4.   Wong-Foy, A. G.; Matzger, A. J.; Yaghi, O. M., Exceptional H_2 saturation uptake in microporous metal− organic frameworks. *J. Am. Chem. Soc.* **2006,** *128* (11), 3494-3495.

5.   Purewal, J.; Liu, D.; Yang, J.; Sudik, A.; Siegel, D.; Maurer, S.; Müller, U., Increased volumetric hydrogen uptake of MOF-5 by powder densification. *Int. J. Hydrogen Energy* **2012,** *37* (3), 2723-2727.

6.   Rowsell, J. L.; Millward, A. R.; Park, K. S.; Yaghi, O. M., Hydrogen sorption in functionalized metal− organic frameworks. *J. Am. Chem. Soc.* **2004,** *126* (18), 5666-5667.

7.   Purewal, J.; Liu, D.; Sudik, A.; Veenstra, M.; Yang, J.; Maurer, S.; Müller, U.; Siegel, D. J., Improved hydrogen storage and thermal conductivity in high-density MOF-5 composites. *J. Phys. Chem. C* **2012,** *116* (38), 20199-20212.

8.   Zacharia, R.; Cossement, D.; Lafi, L.; Chahine, R., Volumetric hydrogen sorption capacity of monoliths prepared by mechanical densification of MOF-177. *J. Mater. Chem.* **2010,** *20* (11), 2145.

9.   Dailly, A.; Poirier, E., Evaluation of an industrial pilot scale densified MOF-177 adsorbent as an on-board hydrogen storage medium. *Energy Environ. Sci.* **2011,** *4* (9), 3527-3534.

10.   Voskuilen, T.; Pourpoint, T.; Dailly, A., Hydrogen adsorption on microporous materials at ambient temperatures and pressures up to 50 MPa. *Adsorption* **2012,** *18*, 239-249.

11.   Purewal, J.; Veenstra, M.; Tamburello, D.; Ahmed, A.; Matzger, A. J.; Wong-Foy, A. G.; Seth, S.; Liu, Y.; Siegel, D. J., Estimation of system-level hydrogen storage for metal-organic frameworks with high volumetric storage density. *Int. J. Hydrogen Energy* **2019,** *44* (29), 15135-15145.

12.   Kapelewski, M. T.; Runčevski, T. e.; Tarver, J. D.; Jiang, H. Z.; Hurst, K. E.; Parilla, P. A.; Ayala, A.; Gennett, T.; FitzGerald, S. A.; Brown, C. M., Record High Hydrogen Storage Capacity in the Metal–Organic Framework Ni$_2$(*m*-dobdc) at Near-Ambient Temperatures. *Chem. Mater.* **2018,** *30* (22), 8179-8189.

13.   Bambalaza, S. E.; Langmi, H. W.; Mokaya, R.; Musyoka, N. M.; Ren, J.; Khotseng, L. E., Compaction of a zirconium metal–organic framework (UiO-66) for high density hydrogen storage applications. *J. Mater. Chem. A* **2018,** *6* (46), 23569-23577.

14.   García-Holley, P.; Schweitzer, B.; Islamoglu, T.; Liu, Y.; Lin, L.; Rodriguez, S.; Weston, M. H.; Hupp, J. T.; Gómez-Gualdrón, D. A.; Yildirim, T., Benchmark study of hydrogen storage in metal–organic frameworks under temperature and pressure swing conditions. *ACS Energy Lett.* **2018,** *3* (3), 748-754.

15.   Blanita, G.; Mihet, M.; Borodi, G.; Misan, I.; Coldea, I.; Lupu, D., Ball milling and compression effects on hydrogen adsorption by MOF:Pt/carbon mixtures. *Microporous Mesoporous Mater.* **2015,** *203*, 195-201.

16.   Geng, Z.; Zhang, C.; Wang, D.; Zhou, X.; Cai, M., Pore size effects of nanoporous carbons with ultra-high surface area on high-pressure hydrogen storage. *J. Energy Chem.* **2015,** *24* (1), 1-8.

17.   Stadie, N. P.; Vajo, J. J.; Cumberland, R. W.; Wilson, A. A.; Ahn, C. C.; Fultz, B., Zeolite-templated carbon materials for high-pressure hydrogen storage. *Langmuir* **2012,** *28*, 10057-10063.

18.   Gabe, A.; Ouzzine, M.; Taylor, E. E.; Stadie, N. P.; Uchiyama, N.; Kanai, T.; Nishina, Y.; Tanaka, H.; Pan, Z.-Z.; Kyotani, T.; Nishihara, H., High-density monolithic pellets of double-sided graphene fragments based on zeolite-templated carbon. *J. Mater. Chem. A* **2021,** *9* (12), 7503-7507.

19.   Chahine, R.; Bose, T., Low-pressure adsorption storage of hydrogen. *Int. J. Hydrogen Energy* **1994,** *19* (2), 161-164.

20.   Streb, A.; Mazzotti, M., Adsorption for efficient low carbon hydrogen production: part 1—adsorption equilibrium and breakthrough studies for $H_2/CO_2/CH_4$ on zeolite 13X. *Adsorption* **2021**, 1-18.

21.   Grazulis, S.; Chateigner, D.; Downs, R. T.; Yokochi, A. F. T.; Quiros, M.; Lutterotti, L.; Manakova, E.; Butkus, J.; Moeck, P.; Le Bail, A., Crystallography Open Database - an open-access collection of crystal structures. *J. Appl. Crystallogr.* **2009,** *42* (4), 726-729.

22.   Baerlocher, C.; McCusker, L. B. Database of Zeolite Structures. http://www.iza-structure.org/databases/.

23.   Taylor, E. E.;   Garman, K.; Stadie, N. P., Atomistic Structures of Zeolite-Templated Carbon. *Chem. Mater.* **2020,** *32* (7), 2742-2752.

24.   Nomura, K.; Nishihara, H.; Yamamoto, M.; Gabe, A.; Ito, M.; Uchimura, M.; Nishina, Y.; Tanaka, H.; Miyahara, M. T.; Kyotani, T., Force-driven reversible liquid–gas phase transition mediated by elastic nanosponges. *Nat. Commun.* **2019,** *10,* 2559.

25.   Willems, T. F.;   Rycroft, C. H.;   Kazi, M.;   Meza, J. C.; Haranczyk, M., Algorithms and tools for high-throughput geometry-based analysis of crystalline porous materials. *Microporous Mesoporous Mater.* **2012,** *149* (1), 134-141.

26.   Bae, Y.-S.;   Yazaydın, A. O. z. r.; Snurr, R. Q., Evaluation of the BET method for determining surface areas of MOFs and zeolites that contain ultra-micropores. *Langmuir* **2010,** *26* (8), 5475-5483.

27.   Casco, M. E.; Martínez-Escandell, M.; Gadea-Ramos, E.; Kaneko, K.; Silvestre-Albero, J.; Rodriguez-Reinoso, F., High-Pressure Methane Storage in Porous Materials: are Carbon Materials in the Pole Position? *Chem. Mater.* **2015**.

28.   Blankenship, T. S.; Mokaya, R., Cigarette butt-derived carbons have ultra-high surface area and unprecedented hydrogen storage capacity. *Energy Environ. Sci.* **2017,** *10* (12), 2552-2562.

29.   Stadie, N. P.;   Purewal, J. J.;   Ahn, C. C.; Fultz, B., Measurements of hydrogen spillover in platinum doped superactivated carbon. *Langmuir* **2010,** *26* (19), 15481-15485.

30.   Nishihara, H.; Hou, P. X.; Li, L. X.; Ito, M.; Uchiyama, M.; Kaburagi, T.; Ikura, A.; Katamura, J.; Kawarada, T.; Mizuuchi, K.; Kyotani, T., High-pressure hydrogen storage in zeolite-templated carbon. *J. Phys. Chem. C* **2009,** *113* (8), 3189-3196.

31.   Ramirez-Vidal, P.; Canevesi, R. L.; Sdanghi, G.; Schaefer, S.; Maranzana, G.;   Celzard, A.; Fierro, V., A Step Forward in Understanding the Hydrogen Adsorption and Compression on Activated Carbons. *ACS Appl. Mater. Inter.* **2021**, *13* (10), 12562–12574.